ACS Photonics

Article

Cite This: ACS Photonics 2018, 5, 3315−3321

Efficient Outcoupling of Organic Light-Emitting Devices Using a Light-Scattering Dielectric Layer

Jongchan Kim,[†] Yue Qu,[†] Caleb Coburn,[‡] and Stephen R. Forrest*[,†,‡,§]

[†]Department of Electrical Engineering and Computer Science, University of Michigan, Ann Arbor, Michigan 48109, United States
[‡]Department of Physics, University of Michigan, Ann Arbor, Michigan 48109, United States
[§]Department of Materials Science and Engineering, University of Michigan, Ann Arbor, Michigan 48109, United States

Supporting Information

ABSTRACT: It has long been a challenge to develop a highly efficient outcoupling method for organic light-emitting diodes that is independent of wavelength and viewing angle, as well as being nonintrusive into the device structure. Here, we demonstrate a transparent, top emitting structure integrated with a high index of refraction waveguide layer and a rough, dielectric diffuse reflector that eliminates plasmonic, waveguide, and substrate modes without introducing wavelength and viewing-angle dependence. The simple outcoupling structure increases the external quantum efficiency from 15 ± 2% to 37 ± 4% compared to an analogous device with a metal mirror, corresponding to a 2.5-fold enhancement without requiring the use of additional outcoupling structures such as microlens arrays or index matching layers to extract substrate modes. The method is potentially suitable for low-cost, solid-state lighting due to its simplicity and high outcoupling efficiency.

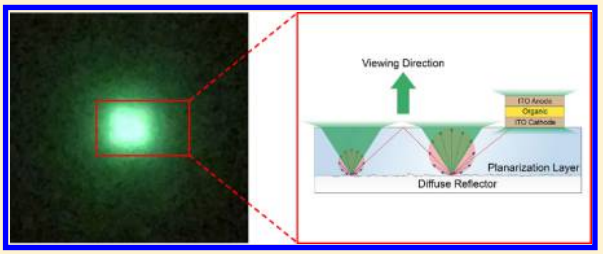

KEYWORDS: *light extraction, phosphorescent OLED, simple process, plasmonic loss*

Phosphorescent organic light-emitting devices (PHOLEDs) can achieve 100% internal quantum efficiency,[1,2] although a considerable amount of light is lost within the device structure[3,4] due to the excitation of substrate,[5,6] waveguide,[7−13] and surface plasmon polariton (SPP) modes,[14−16] as well as absorption in the metal contacts. Substrate modes can be efficiently outcoupled by structuring the air−substrate interface, for example, by using microlens arrays.[17,18] However, reducing loss to waveguide and SPP modes, which is typically >50% in conventional OLEDs, remains a significant hurdle. Several methods such as subanode structures,[7,8,19,20] high refractive index substrates,[21] scattering layers,[5,12,22,23] corrugated structures,[9,24,25] Bragg scatterers,[11,26,27] and microcavities[28] have been demonstrated to overcome these losses, although near-field coupling into SPP modes by the metal electrode is more difficult to avoid.

In particular, top-emitting OLEDs efficiently excite both waveguide and SPP modes due to the strong optical cavity formed between the high-reflectivity semitransparent top electrode and the thick metallic bottom electrode.[29] Several strategies such as thick electron transport layers,[30] metallic grids,[15] and periodically corrugated metal electrodes[11,26,27] suppress the losses. However, these methods are often wavelength and viewing-angle dependent, they are invasive of the device structure, or they are challenging to apply over large substrate areas.

In this work we demonstrate the elimination of SPP modes by replacing the bottom metal electrode in top-emitting OLEDs with a transparent layer of indium tin oxide (ITO) deposited on a polytetrafluoroethylene (PTFE, Teflon) diffuse reflector. The rough reflector surface is planarized by a thick, integrated high index of refraction polymer slab waveguide. The outcoupling of this structure is wavelength and viewing-angle independent. There is no intrusion into the device structure itself since the OLED structure, including the ITO anode, is fabricated on the surface of the planar waveguide. This architecture achieves a 2.5-fold enhancement in outcoupling efficiency compared to an analogous device fabricated on an Al mirror. Simulations indicate that the enhancement can be further increased to 3.4. Importantly, no further light extraction methods such as index matching layers or microlens arrays are required to enhance outcoupling, making this a very simple and potentially low-cost design useful for OLED lighting appliances.

A schematic cross-section of a top-emitting OLED with a PTFE reflector is shown in Figure 1. The surface of the reflector has a root-mean-square roughness of 6.7 μm (measured by profilometry), which is planarized with a transparent polymer waveguide. Light exiting the OLED is either directly emitted from the top surface into the viewing direction or enters the waveguide layer where it propagates until it is incident on the rough reflector surface. There, the light is scattered into a Lambertian profile,[31] and light within the emission cone exits into the viewing direction. Light

Received: April 25, 2018
Published: July 2, 2018

DOI: 10.1021/acsphotonics.8b00539
ACS Photonics 2018, 5, 3315−3321

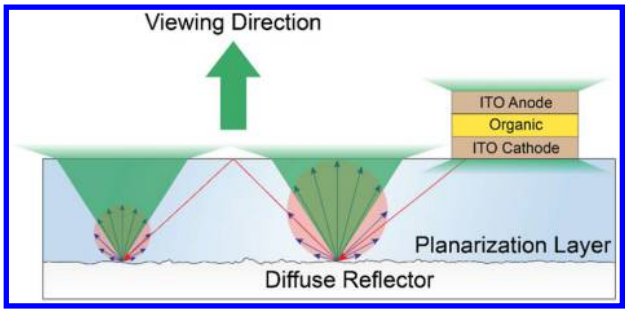

Figure 1. Schematic illustration of the PHOLED on a diffuse reflector. Light incident on the diffuse reflector is scattered into a Lambertian profile (red circles), and light in the emission cone is scattered into the viewing direction (green cone).

incident at angles greater than that for total internal reflection at the polymer−air interface is returned to the diffuse reflector, where it is scattered once again. This repeats until the light is either absorbed or scattered into the viewing direction. As shown in Figure 2a, the PTFE layer has a very low loss even after multiple reflections, enabling multiple iterations of light scattering until the light is extracted.

For an ideal, lossless reflector, the ratio of incident to scattered light power toward the viewing direction from a single diffuse reflection (R_S) is determined using Snell's law, viz., $R_S = (n_{air}/n_P)^2$, where n_{air} and n_P are the refractive indices of the air and waveguide layer, respectively. Then, the ratio of the light intensity extracted into the viewing direction to that within the waveguide layer (η_D) following the path shown in Figure 1 becomes

$$\eta_D = R_S + (1 - R_S)R_S + (1 - R_S)^2 R_S + \ldots = \sum_{n=0}^{\infty} (1 - R_S)^n R_S = 1 \quad (1)$$

In practice, absorption and reflection losses must be taken into account. To quantify the importance of these effects, we use ray tracing to calculate η_D as a function of waveguide layer thickness and absorption coefficient (α), assuming 5% loss at each reflection. As expected, the η_D increases as absorption and reflection losses are reduced; see Figure 2b and c, respectively. The only loss channel in this case is the light propagating to the substrate edge: <0.1% for the $(2.5\ \text{cm})^2$ substrate used in the simulation. As shown in Figure 2c, the primary limit to η_D is the absorption in the waveguide layer.

The outcoupling efficiency (η_{out}) of the OLED is then

$$\eta_{out} = \eta_{TA} + \eta_D \eta_S \quad (2)$$

where η_{TA} is the fraction of light emitted from the top surface and η_S is the fraction of light coupled into the slab waveguide. The simulated[33,34] modal power intensity of both top and bottom OLED emission as a function of the normalized in-plane wave vector $u = k_{||}/(n_{EML}k_0)$ (here $k_{||}$ is the wave vector of the dipole radiation field in the plane of the interface, k_0 is the wave vector in a vacuum, and n_{EML} is the refractive index of the organic layer) of the cavity at different waveguide layer refractive indices (n_P) at the wavelength of λ = 530 nm are shown in Figure 3a and b, respectively. Top emission power propagating with wave vectors $0 < u < n_{air}/n_{EML}$ is emitted into the viewing direction (air modes). Modal power with wave vectors of $n_{air}/n_{EML} < u < n_P/n_{EML}$ is totally internally reflected at the air−top electrode interface. It is subsequently incident

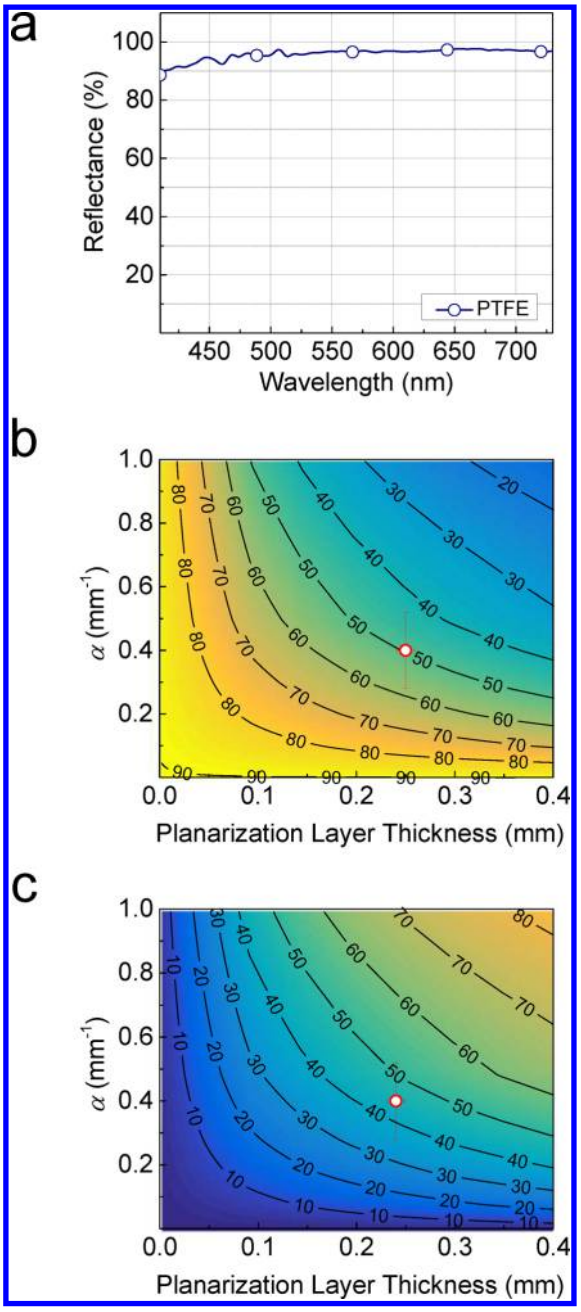

Figure 2. Reflectance and outcoupling efficiency of the diffuser. (a) Reflectance of the PTFE diffuse reflector measured using an integrating sphere. Calculated (b) outcoupling efficiency (η_D) and (c) waveguide layer absorption of the light-diffusing substrate as functions of waveguide thickness and absorption constant (α). The experimental results are indicated as points.

on the waveguide layer (substrate modes). All the bottom emitted power propagating with wave vectors $0 < u < n_P/n_{EML}$ couples into the waveguide. For $n_P/n_{EML} < u < 1$, both top and bottom emission propagates within the OLED active layer. Note that no power exists at $u > 1$, which corresponds to the power coupled into SPP modes. In Figure 3a and b, vertical dashed lines correspond to n_{air}/n_{EML} = 0.55, and n_P/n_{EML} = 0.77, 0.88, and 0.99 for the substrate−waveguide mode boundary at each n_P. For n_P = 1.8, most of the nonradiative modal power propagates within the waveguide layer and is subsequently extracted into the viewing direction via scattering from the rough diffuser interface at the bottom of the polymer

DOI: 10.1021/acsphotonics.8b00539
ACS Photonics 2018, 5, 3315−3321

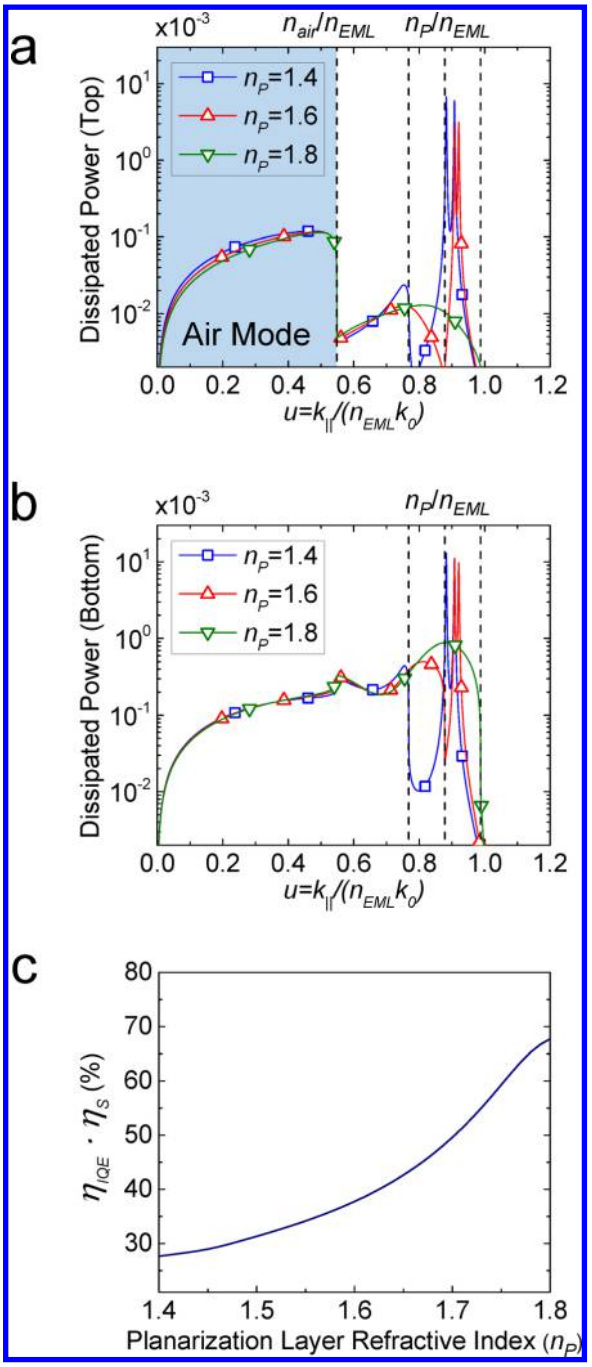

Figure 3. Modal power distribution vs in-plane wave vector for various waveguide layer refractive indices. Simulation of the dissipated optical power of the PHOLED emitted (a) from the top and (b) from the substrate surfaces at a wavelength of 530 nm, i.e., at the emission peak of $Irppy_2acac$ emission. (c) Calculated coupling efficiency into the waveguide layer (η_S) as a function of waveguide layer refractive index (n_P).

waveguide. Figure 3c is a plot of $\eta_{IQE}\eta_S$ vs n_P, with the result that $\eta_{IQE}\eta_S = 67\%$ at $n_P = 1.8$.

To demonstrate the enhancement in external quantum efficiency (η_{EQE}), green and white PHOLEDs with transparent top and bottom contacts were grown on diffuse and metal reflectors. Figure 4a and b are plots of the current density–voltage (J–V) and external quantum efficiency characteristics of the PHOLEDs, respectively (see Methods for structures). The identical J–V characteristics of the PHOLED on the

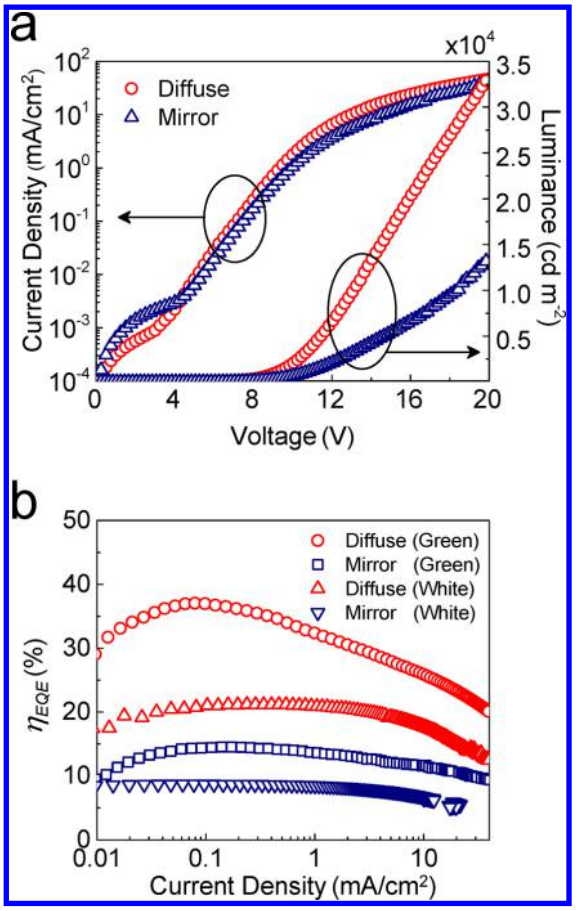

Figure 4. Characteristics of PHOLEDs fabricated on metal mirror and diffuse reflector substrates. (a) Current density–voltage–luminance (J–V–L) characteristics of the green-emitting PHOLED on the two substrates. (b) Current density vs external quantum efficiency (J–η_{EQE}) of the white and green PHOLEDs deposited on metal and diffuse reflecting substrates.

diffuser and the Al mirror show that the flat top surface of the waveguide does not lead to a loss in performance of the subsequently deposited device. The green, diffuse reflecting PHOLED shows a peak $\eta_{EQE} = 37 \pm 4\%$, whereas with a metal mirror, $\eta_{EQE} = 15 \pm 2\%$. A similar enhancement is observed for the white-emitting PHOLED (W-PHOLED), where $\eta_{EQE} = 21 \pm 3\%$ for the diffuse compared with $9 \pm 1\%$ for the metal reflector.

The ability of the diffuse reflector to outcouple guided modes was quantified by comparing its performance with that of a green electrophosphorescent OLED fabricated on a sapphire substrate with a similar refractive index of $n_{saph} = 1.77$ at $\lambda = 530$ nm. The sapphire substrate yields $\eta_{IQE}\eta_{TA} = 7 \pm 2\%$, where η_{IQE} refers to the internal quantum efficiency. Therefore, from eq 2, the light coupled into the waveguide layer shows an outcoupling efficiency of $\eta_{IQE}\eta_S\eta_D = 30 \pm 5\%$ and $8 \pm 3\%$ for the diffuser and metal mirror structures, respectively, resulting in a 3.8 ± 1.5-fold increase in extraction into the viewing direction via diffuse scattering. In Figure 3c, $\eta_{IQE}\eta_S = 67\%$ for $n_P = 1.8$, yielding $\eta_D = 45\%$ and 12% for diffuse and Al mirror substrates, respectively. This corresponds to the ray tracing result in Figure 2b of $\eta_D = 49 \pm 6\%$ for $\alpha = 0.4 \pm 0.1$ mm^{-1} and a thickness of 240 ± 9 μm measured for the waveguide (data point), compared to $\eta_D = 15 \pm 1\%$ for the 20 ± 1 μm

DOI: 10.1021/acsphotonics.8b00539
ACS Photonics 2018, 5, 3315–3321

thick waveguide used for the metal mirror reflector. These results are summarized in Table 1.

Table 1. Modal Power Distribution of Scattering and Specular (Metal) Reflector Substrates

		diffuse reflector		metal reflector
η_{EQE} [a]	37 ± 4%			15 ± 2%
$\eta_{IQE}\eta_{TA}$ [b]	7 ± 2%			7 ± 2%
$\eta_{IQE}\eta_S\eta_D$	active area	14 ± 5%	30 ± 5%	8 ± 3%
	periphery	16 ± 2%		
η_S [a]	67%			67%
η_D [c]	45% (49%)			12% (15%)

[a]Measured. [b]Calculated based on Green's function analysis. [c]Combined result from experiment and Green's function analysis. The result in parentheses is from ray tracing analysis.

The diffuser increases the étendue of the system, thus introducing emission outside of the PHOLED active area defined by the device contacts. Figure 5a and b show the normalized radiated power intensities from the PHOLED deposited on a diffuse reflector and Al mirror, respectively. The calculations assume α = 0.4 mm^{-1}, a 1 mm^2 device area, and waveguide layer thicknesses of 240 and 20 μm for the diffuser and Al mirror, respectively. The black dashed lines define the device contact area. Photographic images of emission from PHOLEDs on each substrate are shown in Figure 5c and d, insets, showing similar behavior to the simulation. The redirection of the incident rays from the diffuse reflector isotropically redistributes the power, thus showing a circular emission pattern. Thinner waveguide layers suppress this effect due to the smaller subtended area. Contrary to the diffuse reflector, the specular reflection of the Al mirror does not affect the azimuthal ray direction, maintaining the defined device appearance.

To investigate the fraction of the peripheral emission from the PHOLED using the diffuser layer, we measured its intensity profile following the trajectory of the dashed lines in Figure 5a and b, with the results given in Figure 5c and d along with a fit using ray tracing. The index of refraction at the top surface of the optical cavity changes from the ITO contact (n_{ITO} = 2.1) to the waveguide layer (n_p = 1.8), resulting in the emission peaks at the device edges in Figure 5d. Integrating the radiated power outside the device active area indicates that 54% of the total emission is emitted beyond the contact periphery for the diffuser, whereas the Al mirror substrate showed <10% of emission from the periphery. As expected, the fraction of peripheral emission decreases with device area.

We simulated η_D of OLEDs whose areas cover a large fraction of the substrate size (25 mm^2), which is the common

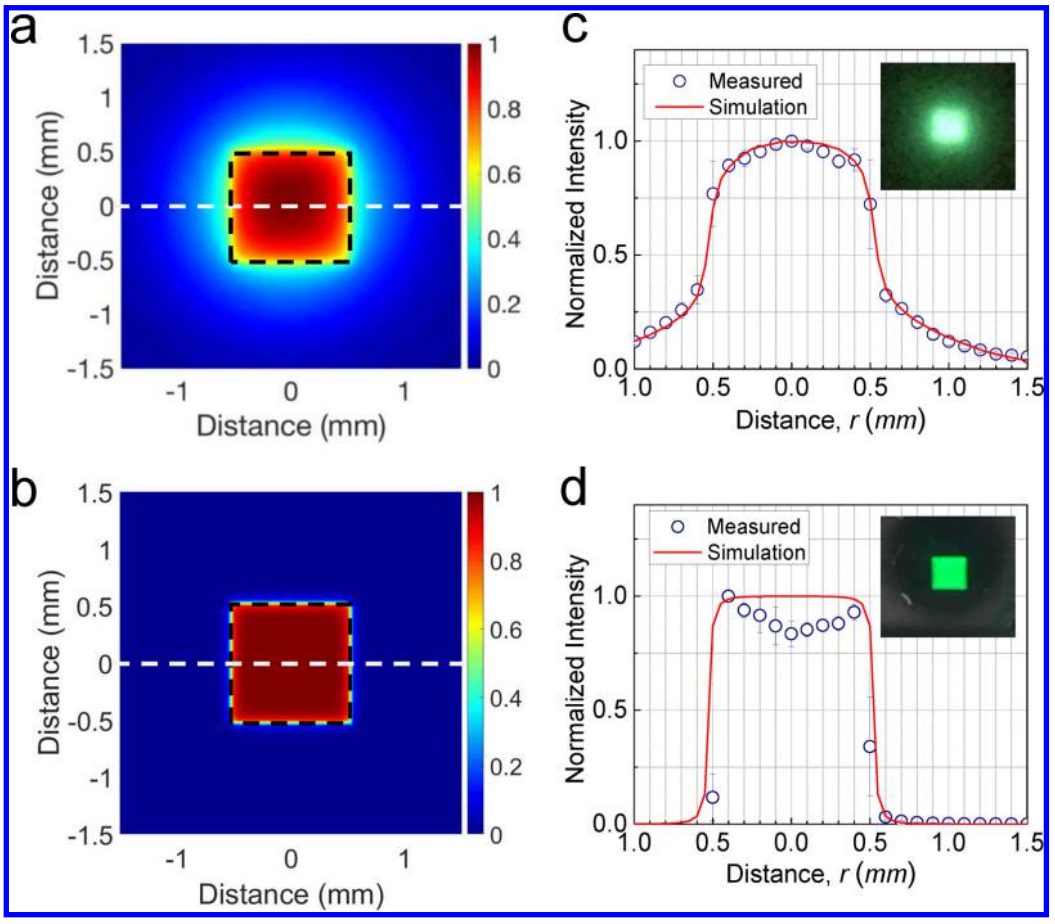

Figure 5. Radiant power intensity profile for PHOLEDs on diffuse reflector and Al mirror substrates. (a) Simulated radiant power for a PHOLED on a diffuse reflector substrate. The white dashed line shows the measurement trajectory for (c). The black dashed line indicates the device active area. (b) Simulated radiant power for the PHOLED on a specular (metal mirror) substrate. (c, d) Measured (circles) radial peak intensity profiles along the white dashed line bisecting the PHOLED in (a) and (b) along with the ray tracing fit (lines). Insets: Photographs of emission from the green PHOLED deposited on each substrate.

DOI: 10.1021/acsphotonics.8b00539
ACS Photonics 2018, 5, 3315−3321

situation found in actual lighting panels. The results of the simulation are provided in Supporting Information, Figure S1. We find that η_D is unchanged for device areas of <20 mm^2. At >20 mm^2, η_D was reduced due to the waveguided emission reaching the substrate edge, although the effects were ≤2%. The fraction of peripheral emission decreases with increased device area, resulting in the loss of only an insignificant fraction of the light in the waveguide layer at the substrate edge for large-area devices.

The spectrum of a conventional PHOLED depends on viewing angle due to weak optical microcavity effects.[3] Bulović et al.[3] measured the angular distribution of the radiant intensity and showed that the spectral shift in a green OLED is approximately 30−40 nm, depending on the device structure. Cavity effects are more pronounced for top-emitting OLEDs due to the large difference in the refractive index between the transparent ITO top contact and air. This effect is especially critical for white light sources due to their broad spectra. The use of a high refractive index waveguide layer suppresses spectral shifts at large viewing angles,[20] thus reducing cavity effects. As a result, the spectra of the devices on both the mirror and the diffuse reflector substrates are independent of viewing angle, as shown in Figure 6a. The spectrum of the device on the mirror substrate measured perpendicular to the substrate (0°) shows Fabry−Perot resonances due to the interference within the waveguide layer. Light scattering into all directions by the diffuse reflector eliminates the resonances. Furthermore, scattering by the diffuse reflector results in a Lambertian emission profile, shown in Figure 6b.

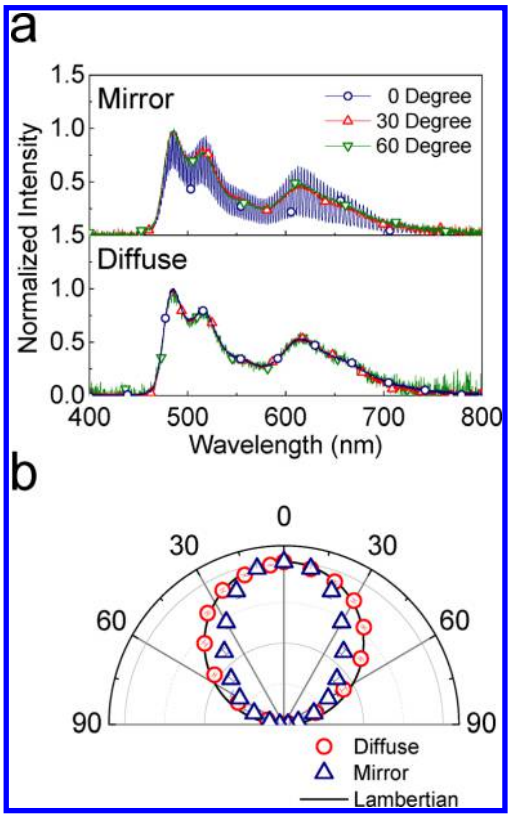

Figure 6. Emission profiles of the white PHOLED. (a) White PHOLED emission spectrum at viewing angles of 0°, 30°, and 60°. (b) Polar plot of the peak intensity. The solid line indicates a Lambertian profile.

The thickness of the waveguide affects the power lost via absorption. The ray tracing simulations show that η_D can approach 75% for a 50 μm thick waveguide layer at α = 0.4 mm^{-1}, leading to η_{EQE} = 68% with 100% device internal quantum efficiency. From this we infer a 3.4-fold enhancement compared to the substrate with the metal mirror. The emission profile also depends on the waveguide layer thickness. This results since more reflections occur during lateral propagation in a thinner waveguide layer. A 50 μm waveguide layer is expected to show a peripheral emission of 13%.

Since power coupled into nonradiative modes is not viewable, outcoupling schemes fall into two categories: concentrating power into air modes[28] or redirecting the wave vectors of the nonradiative modes. A means for redirecting the wave vector is via scattering,[7,8,25,26] which provides a route to reduce the in-plane momentum from $n_{air}/n_{EML} < u < 1$ to $0 < u < n_{air}/n_{EML}$. The Lambertian profile of the diffuse reflector shows that it evenly redistributes the incident power for each wave vector. Figure 7a shows the variation in modal power distribution vs the number of reflections in the waveguide layer. At each reflection the power confined in the waveguide layer ($n_{air}/n_P < u < 1$) is redistributed into all wave vectors, where wave vectors of $0 < u < n_{air}/n_P$ are extracted into the viewing direction. Thus, the power confined within the waveguide layer decreases as the wave propagates. The

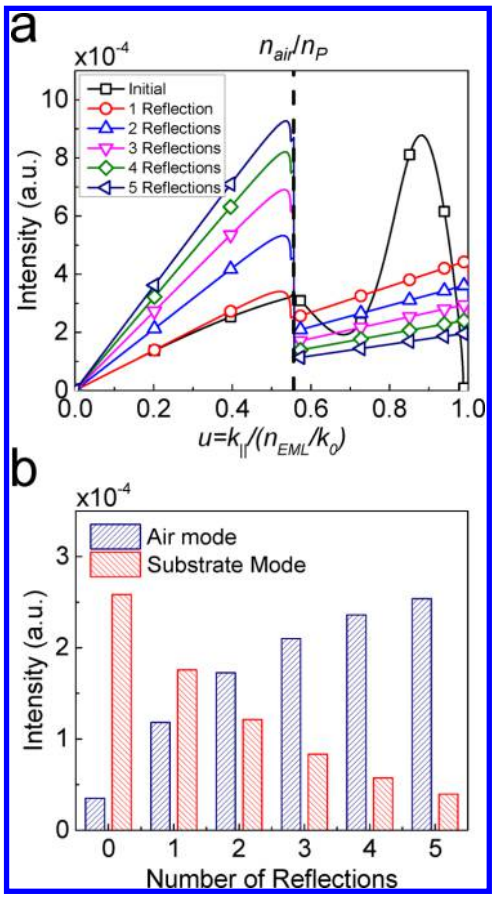

Figure 7. Modal power distribution evolution with number of reflections. (a) Modal power distribution vs the number of reflections in the waveguide layer. The dashed line represents the boundary between air and substrate modes at $u = n_{air}/n_P$. (b) Distribution of modal power in air and substrate modes following each reflection.

DOI: 10.1021/acsphotonics.8b00539
ACS Photonics 2018, 5, 3315−3321

integrated modal power of air and substrate modes is given in Figure 7b.

A number of scattering methods redirect only a fraction of the scattered light into the viewing direction, and hence in those approaches, an outcoupling efficiency similar to that achieved here requires further enhancements by using microlens arrays or index matching fluid (Table S2 for performance of different outcoupling schemes). In addition, the coupling into SPP modes and absorption by metal cathodes lead to additional losses, preventing wave propagation over long distances. The use of a diffuse reflector with a transparent OLED completely prevents coupling into these loss channels. Therefore, efficient outcoupling is possible using only the diffuser and waveguide, making it considerably simpler and less costly to implement.

In conclusion, we demonstrate an efficient, transparent top-emitting structure with a diffuse reflector planarized by a transparent slab waveguide. The diffuse reflector eliminates losses due to coupling to SPP modes, while redirecting the laterally propagating light within the waveguide layer into the viewing direction. The planarizing polymer with a high refractive index (n_P = 1.8) is deposited onto the diffuse reflector surface to maximize the light coupled into the diffuser, as well as to create a smooth surface on which to fabricate the PHOLED. The device on the diffuse reflector showed 2.5-fold enhancement in external quantum efficiency compared to an analogous PHOLED on a metal mirror. The architecture does not require additional outcoupling structures such as microlens arrays to enhance the outcoupling efficiency. The diffuse reflector shows no wavelength or viewing angle dependence, exhibiting a Lambertian emission profile. Our results provide a simple solution at a potentially low cost for OLED lighting applications.

METHODS

Substrate Preparation. The PTFE reflector (Spectralex, Lake-Photonics GmbH) was exposed to UV-ozone for 20 min prior to coating by the polymer waveguide (NOA 170, Norland Products, Inc.). A flat (root-mean-square roughness <0.5 nm) polydimethylsiloxane stamp attached onto a glass handle was pressed onto the polymer on the diffuser surface for planarization, during which it was exposed to UV light for 220 s prior to stamp removal. The metal mirror substrate was fabricated by depositing a 100 nm thick Al mirror on the glass substrate followed by spin coating the polymer waveguide at 3000 rpm on its surface. Then the polymer was exposed to UV light as above.

Device Fabrication. A 50 nm thick ITO cathode (bottom electrode) was deposited on the smooth polymer surface using Ar plasma sputter deposition at 5 mTorr. The active regions of the PHOLEDs were grown by vacuum thermal evaporation at a base pressure of 10^{-7} Torr. The green transparent PHOLED comprised bathophenanthroline (BPhen):Li 20 nm/BPhen 40 nm/4,4′-bis(*N*-carbazolyl)-1,1′-biphenyl (CBP):bis(2-phenylpyridine)(acetylacetonate)Ir(III)($Irppy_2$acac) 30 nm/4,4′-cyclohexylidenebis[*N*,*N*-bis(4-methylphenyl)-benzenamine] (TAPC) 60 nm/TAPC:MoO_3 30 nm. This was capped with a sputter-deposited, 50 nm thick top ITO anode using similar conditions to those of the cathode. The same structure was simultaneously deposited on both metal mirror and diffuse reflector substrates.

The white PHOLED comprised BPhen:Li 40 nm/3,3′,5,5′-tetra[(*m*-pyridyl)phen-3-yl]biphenyl (BP4mPy) 15 nm/CBP:bis[2-(4,6-difluorophenyl)pyridinato-*C*2,*N*](picolinato)-Ir(III)(FIrpic) 10 nm/CBP:$Irppy_2$acac:bis(2-methyldibenzo-quinoxaline)(acetylacetonate)Ir(III) ($IrMDQ_2$acac) 15 nm/TAPC 20 nm/TAPC:MoO_3 30 nm/thick ITO 50 nm. The devices were patterned using a shadow mask of an array of 1 mm strips, resulting in a crossbar of top and bottom ITO contacts that defined the 1 mm × 1 mm device active area.

Device and Reflector Characterization. The current density−voltage characteristics of the PHOLEDs were measured using a parameter analyzer (HP4145, Hewlett-Packard) and a calibrated photodiode (S3584-08, Hamamatsu Photonics) following standard procedures.[32] The emission spectra at J = 10 mA cm^{-2} were measured using a spectrometer (USB2000, Ocean Optics, Inc.) connected to the device via an optical fiber (P400-5-UV-vis, Ocean Optics, Inc.). The reflectance from the PTFE diffuse reflector was measured in an integrating sphere. A spectrometer was used to measure the spectrum of the excitation light source (OSL1, Fiber Illuminator, Thorlabs, Inc.) connected to the integrating sphere with and without the sample present. The spectra were compared to obtain the sample reflectance. Angle-dependent emission spectra were measured by placing the substrate perpendicular to the plane of detection and positioning the detector on a motorized rotational stage.

Device Simulation. The modal power distribution of the PHOLED was calculated based on Green's function analysis.[33,34] The device structure used for the simulation is ITO 50 nm/BPhen 60 nm/CBP 30 nm (active layer)/TAPC 90 nm/ITO 50 nm/waveguide layer. We used the refractive indices at λ = 530 nm, corresponding to the peak wavelength for $Irppy_2$acac emission. The dipole orientation of $Irppy_2$acac (θ = 0.23) was included in the simulations,[35] and the emitter location was assumed to be in the center of the EML. The 16% electrical loss in internal quantum efficiency, obtained from the fit of the top emission from the OLED on the sapphire substrate, was used for the analysis in Figure 3c. The light within the substrate was calculated using the Monte Carlo ray tracing method. Calculation details are included in Figure S3. Refractive indices for all materials were measured using variable-angle spectroscopic ellipsometry (Figure S4).

ASSOCIATED CONTENT

Supporting Information

The Supporting Information is available free of charge on the ACS Publications website at DOI: 10.1021/acsphotonics.8b00539.

Additional information (PDF)

AUTHOR INFORMATION

Corresponding Author

*E-mail: stevefor@umich.edu.

ORCID

Stephen R. Forrest: 0000-0003-0131-1903

Notes

The authors declare the following competing financial interest(s): S.R.F. has an equity interest in Universal Display Corp. This apparent conflict is under management by the University of Michigan Office of Research.

DOI: 10.1021/acsphotonics.8b00539
ACS Photonics 2018, 5, 3315−3321

■ ACKNOWLEDGMENTS

The work was supported by the U.S. Department of Energy, Office of Energy Efficiency and Renewable Energy (EERE), and Universal Display Corp. We thank Byungjun Lee, Chanho Soh, Dejiu Fan, and Xinhong Du for helpful discussions.

■ REFERENCES

(1) Baldo, M. A.; O'Brien, D. F.; You, Y.; Shoustikov, A.; Sibley, S.; Thompson, M. E.; Forrest, S. R. Highly Efficient Phosphorescent Emission from Organic Electroluminescent Devices. *Nature* **1998**, *395* (6698), 151−154.

(2) Baldo, M. A.; Lamansky, S.; Burrows, P. E.; Thompson, M. E.; Forrest, S. R. Very High-Efficiency Green Organic Light-Emitting Devices Based on Electrophosphorescence. *Appl. Phys. Lett.* **1999**, *75* (1), 4−6.

(3) Bulović, V.; Khalfin, V. B.; Gu, G.; Burrows, P. E.; Garbuzov, D. Z.; Forrest, S. R. Weak Microcavity Effects in Organic Light-Emitting Devices. *Phys. Rev. B: Condens. Matter Mater. Phys.* **1998**, *58* (7), 3730−3740.

(4) Brütting, W.; Frischeisen, J.; Schmidt, T. D.; Scholz, B. J.; Mayr, C. Device Efficiency of Organic Light-Emitting Diodes: Progress by Improved Light Outcoupling. *Phys. Status Solidi A* **2013**, *210* (1), 44−65.

(5) Koh, T.-W.; Spechler, J. A.; Lee, K. M.; Arnold, C. B.; Rand, B. P. Enhanced Outcoupling in Organic Light-Emitting Diodes via a High-Index Contrast Scattering Layer. *ACS Photonics* **2015**, *2* (9), 1366−1372.

(6) Lee, K. M.; Fardel, R.; Zhao, L.; Arnold, C. B.; Rand, B. P. Enhanced Outcoupling in Flexible Organic Light-Emitting Diodes on Scattering Polyimide Substrates. *Org. Electron.* **2017**, *51*, 471−476.

(7) Sun, Y.; Forrest, S. R. Enhanced Light out-Coupling of Organic Light-Emitting Devices Using Embedded Low-Index Grids. *Nat. Photonics* **2008**, *2* (8), 483−487.

(8) Qu, Y.; Slootsky, M.; Forrest, S. R. Enhanced Light Extraction from Organic Light-Emitting Devices Using a Sub-Anode Grid. *Nat. Photonics* **2015**, *9* (11), 758−763.

(9) Koo, W. H.; Jeong, S. M.; Araoka, F.; Ishikawa, K.; Nishimura, S.; Toyooka, T.; Takezoe, H. Light Extraction from Organic Light-Emitting Diodes Enhanced by Spontaneously Formed Buckles. *Nat. Photonics* **2010**, *4* (4), 222−226.

(10) Zhou, L.; Ou, Q.-D.; Chen, J.-D.; Shen, S.; Tang, J.-X.; Li, Y.-Q.; Lee, S.-T. Light Manipulation for Organic Optoelectronics Using Bio-Inspired Moth's Eye Nanostructures. *Sci. Rep.* **2015**, *4*, DOI: 10.1038/srep04040.

(11) Bocksrocker, T.; Preinfalk, J. B.; Asche-Tauscher, J.; Pargner, A.; Eschenbaum, C.; Maier-Flaig, F.; Lemme, U. White Organic Light Emitting Diodes with Enhanced Internal and External Outcoupling for Ultra-Efficient Light Extraction and Lambertian Emission. *Opt. Express* **2012**, *20* (S6), A932.

(12) Chang, H.-W.; Lee, J.; Hofmann, S.; Hyun Kim, Y.; Müller-Meskamp, L.; Lüssem, B.; Wu, C.-C.; Leo, K.; Gather, M. C. Nano-Particle Based Scattering Layers for Optical Efficiency Enhancement of Organic Light-Emitting Diodes and Organic Solar Cells. *J. Appl. Phys.* **2013**, *113* (20), 204502.

(13) Lee, J.; Han, T.-H.; Park, M.-H.; Jung, D. Y.; Seo, J.; Seo, H.-K.; Cho, H.; Kim, E.; Chung, J.; Choi, S.-Y.; et al. Synergetic Electrode Architecture for Efficient Graphene-Based Flexible Organic Light-Emitting Diodes. *Nat. Commun.* **2016**, *7*, 11791.

(14) Nowy, S.; Krummacher, B. C.; Frischeisen, J.; Reinke, N. A.; Brütting, W. Light Extraction and Optical Loss Mechanisms in Organic Light-Emitting Diodes: Influence of the Emitter Quantum Efficiency. *J. Appl. Phys.* **2008**, *104* (12), 123109.

(15) Qu, Y.; Coburn, C.; Fan, D.; Forrest, S. R. Elimination of Plasmon Losses and Enhanced Light Extraction of Top-Emitting Organic Light-Emitting Devices Using a Reflective Subelectrode Grid. *ACS Photonics* **2017**, *4* (2), 363−368.

(16) Hobson, P. A.; Wedge, S.; Wasey, J. A. E.; Sage, I.; Barnes, W. L. Surface Plasmon Mediated Emission from Organic Light-Emitting Diodes. *Adv. Mater.* **2002**, *14* (19), 1393−1396.

(17) Sun, Y.; Forrest, S. R. Organic Light Emitting Devices with Enhanced Outcoupling via Microlenses Fabricated by Imprint Lithography. *J. Appl. Phys.* **2006**, *100* (7), 73106.

(18) Kim, J.-J.; Lee, J.; Yang, S.-P.; Kim, H. G.; Kweon, H.-S.; Yoo, S.; Jeong, K.-H. Biologically Inspired Organic Light-Emitting Diodes. *Nano Lett.* **2016**, *16* (5), 2994−3000.

(19) Slootsky, M.; Forrest, S. R. Enhancing Waveguided Light Extraction in Organic LEDs Using an Ultra-Low-Index Grid. *Opt. Lett.* **2010**, *35* (7), 1052−1054.

(20) Qu, Y.; Kim, J.; Coburn, C.; Forrest, S. R. Efficient, Nonintrusive Outcoupling in Organic Light Emitting Devices Using Embedded Microlens Arrays. *ACS Photonics* **2018**, *5*, 2453.

(21) Mladenovski, S.; Neyts, K.; Pavicic, D.; Werner, A.; Rothe, C. Exceptionally Efficient Organic Light Emitting Devices Using High Refractive Index Substrates. *Opt. Express* **2009**, *17* (9), 7562−7570.

(22) Jeon, S.; Lee, S.; Han, K.-H.; Shin, H.; Kim, K.-H.; Jeong, J.-H.; Kim, J.-J. High-Quality White OLEDs with Comparable Efficiencies to LEDs. *Adv. Opt. Mater.* **2018**, *6* (8), 1701349.

(23) Tang, Z.; Elfwing, A.; Bergqvist, J.; Tress, W.; Inganäs, O. Light Trapping with Dielectric Scatterers in Single- and Tandem-Junction Organic Solar Cells. *Adv. Energy Mater.* **2013**, *3* (12), 1606−1613.

(24) Kim, J. B.; Kim, P.; Pégard, N. C.; Oh, S. J.; Kagan, C. R.; Fleischer, J. W.; Stone, H. A.; Loo, Y.-L. Wrinkles and Deep Folds as Photonic Structures in Photovoltaics. *Nat. Photonics* **2012**, *6* (5), 327−332.

(25) Ou, Q.; Zhou, L.; Li, Y.; Shen, S.; Chen, J.-D.; Li, C.; Wang, Q.-K.; Lee, S.; Tang, J. Extremely Efficient White Organic Light-Emitting Diodes for General Lighting. *Adv. Funct. Mater.* **2014**, *24* (46), 7249−7256.

(26) Wedge, S.; Giannattasio, A.; Barnes, W. L. Surface Plasmon−polariton Mediated Emission of Light from Top-Emitting Organic Light-Emitting Diode Type Structures. *Org. Electron.* **2007**, *8* (2−3), 136−147.

(27) Bi, Y.-G.; Feng, J.; Liu, Y.-S.; Li, Y.-F.; Chen, Y.; Zhang, X.-L.; Han, X.-C.; Sun, H.-B. Surface Plasmon-Polariton Mediated Red Emission from Organic Light-Emitting Devices Based on Metallic Electrodes Integrated with Dual-Periodic Corrugation. *Sci. Rep.* **2015**, *4*, 7108.

(28) Wang, Z. B.; Helander, M. G.; Qiu, J.; Puzzo, D. P.; Greiner, M. T.; Hudson, Z. M.; Wang, S.; Liu, Z. W.; Lu, Z. H. Unlocking the Full Potential of Organic Light-Emitting Diodes on Flexible Plastic. *Nat. Photonics* **2011**, *5* (12), 753−757.

(29) Hofmann, S.; Thomschke, M.; Lüssem, B.; Leo, K. Top-Emitting Organic Light-Emitting Diodes. *Opt. Express* **2011**, *19* (106), A1250−A1264.

(30) Meerheim, R.; Furno, M.; Hofmann, S.; Lüssem, B.; Leo, K. Quantification of Energy Loss Mechanisms in Organic Light-Emitting Diodes. *Appl. Phys. Lett.* **2010**, *97* (25), 253305.

(31) van Ginneken, B.; Stavridi, M.; Koenderink, J. J. Diffuse and Specular Reflectance from Rough Surfaces. *Appl. Opt.* **1998**, *37* (1), 130−139.

(32) Forrest, S. R.; Bradley, D. D. C.; Thompson, M. E. Measuring the Efficiency of Organic Light-Emitting Devices. *Adv. Mater.* **2003**, *15* (13), 1043−1048.

(33) Celebi, K.; Heidel, T. D.; Baldo, M. A. Simplified Calculation of Dipole Energy Transport in a Multilayer Stack Using Dyadic Green's Functions. *Opt. Express* **2007**, *15* (4), 1762−1772.

(34) Chance, R. R.; Prock, A.; Silbey, R. Lifetime of an Emitting Molecule near a Partially Reflecting Surface. *J. Chem. Phys.* **1974**, *60* (7), 2744−2748.

(35) Graf, A.; Liehm, P.; Murawski, C.; Hofmann, S.; Leo, K.; Gather, M. C. Correlating the Transition Dipole Moment Orientation of Phosphorescent Emitter Molecules in OLEDs with Basic Material Properties. *J. Mater. Chem. C* **2014**, *2* (48), 10298−10304.

DOI: 10.1021/acsphotonics.8b00539
ACS Photonics 2018, 5, 3315−3321